

Origin, fate and dynamics of macrophages at central nervous system interfaces

Tobias Goldmann^{1,14}, Peter Wieghofer^{1,2,14}, Marta Joana Costa Jordão^{1,2,14}, Fabiola Prutek¹, Nora Hagemeyer¹, Kathrin Frenzel^{1,2}, Lukas Amann^{1,2}, Ori Staszewski¹, Katrin Kierdorf¹, Martin Krueger³, Giuseppe Locatelli⁴, Hannah Hochgerner⁵, Robert Zeiser^{6,7}, Slava Epelman⁸, Frederic Geissmann⁹, Josef Priller¹⁰, Fabio M V Rossi¹¹, Ingo Bechmann³, Martin Kerschensteiner^{4,12}, Sten Linnarsson⁵, Steffen Jung¹³ & Marco Prinz^{1,7}

Perivascular, subdural meningeal and choroid plexus macrophages are non-parenchymal macrophages that mediate immune responses at brain boundaries. Although the origin of parenchymal microglia has recently been elucidated, much less is known about the precursors, the underlying transcriptional program and the dynamics of the other macrophages in the central nervous system (CNS). It was assumed that they have a high turnover from blood-borne monocytes. However, using parabiosis and fate-mapping approaches in mice, we found that CNS macrophages arose from hematopoietic precursors during embryonic development and established stable populations, with the notable exception of choroid plexus macrophages, which had dual origins and a shorter life span. The generation of CNS macrophages relied on the transcription factor PU.1, whereas the MYB, BATF3 and NR4A1 transcription factors were not required.

Under steady-state conditions, the CNS hosts a heterogeneous population of myeloid cells, including parenchymal microglia and non-parenchymal perivascular, subdural meningeal and choroid plexus macrophages^{1–3}. The latter myeloid cells are critical effectors and regulators of immune responses at CNS borders during virtually all neuroinflammatory, neurodegenerative and neuro-oncological diseases.

Unlike microglia, which are derived from early yolk sac precursors before birth^{4–7}, all other CNS macrophages found in the perivascular (Virchow-Robin) spaces, subdural meninges and choroid plexus were believed to originate from short-lived blood monocytes after birth that are quickly replaced by bone marrow (BM)-derived cells^{3,8}. These assumptions were made on the basis of cell transplantation experiments in rodents starting in the 1980s (refs. 9,10). Subsequently, chemotherapeutic conditioning also suggested that perivascular macrophages were present in the CNS parenchyma after BM transplantation^{11,12}. However, all of these studies used either irradiation or chemotherapy as conditioning regimens, thereby inducing an artificial influx of injected BM-derived cells, likely as a result of changes of the blood-brain barrier and local induction of chemoattractants in the host CNS^{13–15}.

Thus, it has been believed for decades that microglia and non-parenchymal macrophages in the subdural meninges, perivascular spaces and choroid plexus represent two ontogenetically and

transcriptionally distinct myeloid populations. By combining large-scale single-cell RNA-sequencing with multiple approaches of fate-mapping, parabiosis and *in vivo* imaging, we challenged the view that non-parenchymal macrophages are BM derived and provide new insights into the transcriptional networks, ancestry and turnover of these macrophages at CNS boundaries. We also found that non-parenchymal CNS macrophages are closely related to microglia, but still represent a distinct specialized population of tissue macrophages.

RESULTS

Gene expression profiling of CNS macrophages

Myeloid cells in the brain are a diverse group of cells localized at strategic places of the CNS. The parenchyma is populated with microglia, whereas tissue borders host Iba-1⁺ macrophages that can be found in the subdural meninges (mMΦ), perivascular spaces (pvMΦ) and choroid plexus (cpMΦ) (Fig. 1a).

CNS macrophages have historically been classified on the basis of their distinct anatomical localization, morphology and expression of selected molecular markers¹. In detail, pvMΦ have been described to express CD206, a receptor on non-parenchymal macrophages in the CNS and to be sandwiched between the laminin-positive endothelial and glial basement membranes¹⁶. In contrast, subdural mMΦ are

¹Institute of Neuropathology, Freiburg University Medical Centre, Freiburg, Germany. ²Faculty of Biology, University of Freiburg, Freiburg, Germany. ³Institute of Anatomy, University of Leipzig, Leipzig, Germany. ⁴Institut für Klinische Neuroimmunologie, Ludwig-Maximilians Universität München, Munich, Germany. ⁵Division of Molecular Neurobiology, Department of Medical Biochemistry and Biophysics, Karolinska Institutet, Stockholm, Sweden. ⁶Department of Hematology and Oncology, Freiburg University Medical Centre, Freiburg, Germany. ⁷BIOSS Centre for Biological Signaling Studies, University of Freiburg, Freiburg, Germany. ⁸Peter Munk Cardiac Centre, University Health Network Toronto, Ontario, Canada. ⁹Centre for Molecular and Cellular Biology of Inflammation, King's College London, London, UK. ¹⁰Department of Neuropsychiatry and Laboratory of Molecular Psychiatry, Charité – Universitätsmedizin Berlin; Cluster of Excellence NeuroCure, DZNE & BIH, Berlin, Germany. ¹¹The Biomedical Research Centre, Faculty of Medicine, University of British Columbia, Vancouver, British Columbia, Canada. ¹²Munich Cluster for Systems Neurology (SyNergy), Munich, Germany. ¹³Department of Immunology, The Weizmann Institute of Science, Rehovot, Israel. ¹⁴These authors contributed equally to this work. Correspondence should be addressed to M.P. (marco.prinz@uniklinik-freiburg.de).

Received 20 August 2015; accepted 1 March 2016; published online 2 May 2016; doi:10.1038/ni.3423

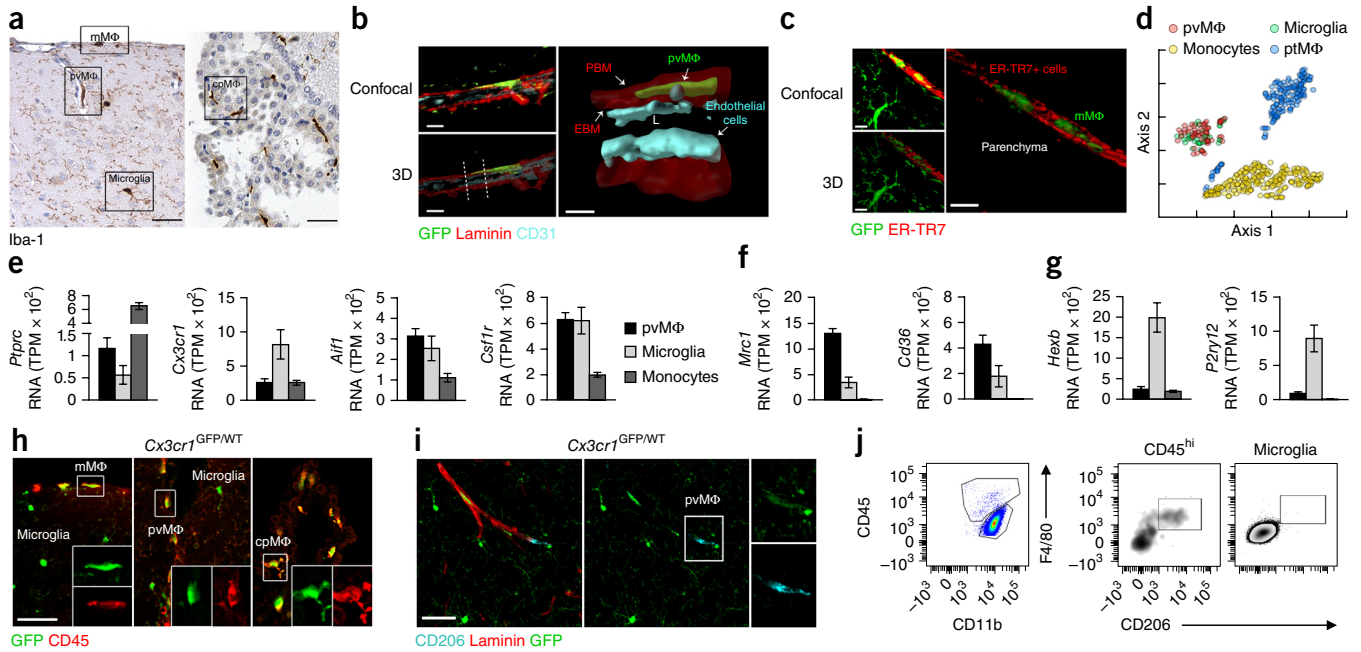


Figure 1 Molecular census of non-parenchymal macrophages, microglia and monocytes. (a) Iba-1 immunohistochemistry for mMΦ, pvMΦ, cpMΦ and microglia. Scale bars represent 50 μ m. (b) Confocal microscopy and three-dimensional reconstruction of a CD31⁺ (cyan) cerebral blood vessel and CX₃CR1-GFP⁺ (green) pvMΦ in the perivascular space (laminin⁺, red; parenchymal basement membranes, PBM; endothelial basement membrane, EBM). Dashed lines indicate the cross section shown at the right. Scale bars, 10 μ m (left) and 3 μ m (right). (c) Confocal image and three-dimensional reconstruction of CX₃CR1-GFP⁺ (green) mMΦ. mMΦ were localized in ER-TR7⁺ (red) fibroblasts. Scale bars, 10 μ m (left) and 3 μ m (right). (d) Cluster analysis using t-SNE of individual cortical pvMΦ, cortical microglia, ptMΦ and monocytes were measured by single-cell RNA sequencing and bi-clustering. (e–g) Single-cell RNA-seq analysis of mRNA encoding selected markers for individual cells that were either commonly (e) or highly expressed in pvMΦ (f) or in microglia, respectively (g). (h) Immunofluorescence of GFP (CX₃CR1, green) and CD45 (red) in the brain of adult *Cx3cr1*^{GFP/WT} mice demonstrating CD45 on pvMΦ, cpMΦ and mMΦ, but not on microglia. Scale bar, 25 μ m. (i) Immunofluorescence of CD206 (cyan), GFP (CX₃CR1, green) and laminin (BM, red) showing the selective expression of CD206 by pvMΦ. Scale bar, 50 μ m. (j) Gating of CD11b⁺CD45^{hi}CD206⁺ MΦ and CD11b⁺CD45^{lo}CD206⁻ microglia cells isolated from the cortex (without meninges and choroid plexus) pre-gated on CD45⁺CD11b⁺Ly6C⁻Ly6G⁻. (k) Flow cytometry of cortical pvMΦ and microglia. Mean fluorescence intensity (MFI) of CD45, CD206, CD36 and F4/80. Data are from two independent experiments with four mice (a–c), three mice (h–j) or six biological replicates (k; mean \pm s.e.m.) or two independent experiments with 167 ptMΦ, 246 monocytes, 33 microglia and 65 pvMΦ (d–g; mean \pm s.e.m. in e–g).

localized in close vicinity to ER-TR7⁺ fibroblast-like cells that line the meninges and meningeal vasculature¹⁷. Finally, cpMΦ are found exclusively in the stroma and epithelial layer of the choroid plexus. Using confocal microscopy and subsequent three-dimensional reconstruction of brain tissue from mice in which one allele of the gene encoding the cytokine receptor CX₃CR1 contains the gene encoding GFP (*Cx3cr1*^{GFP/WT}), we were able to accordingly identify Iba-1⁺CX₃CR1⁺ pvMΦ on the basis of their close proximity to the abluminal side of endothelial cells (CD31⁺) between the endothelial and the parenchymal basement membrane (laminin⁺), the perivascular space (Fig. 1b). In the subdural meninges, we localized Iba-1⁺CX₃CR1⁺ mMΦ by their close proximity to fibroblasts expressing ER-TR7 (Fig. 1c).

We then used an unbiased, surface marker-free approach to thoroughly molecularly characterize cortical microglia and cortical pvMΦ. For that purpose, we prepared a whole-cortex cell suspension devoid of meninges and choroid plexus. We then performed unbiased quantitative single-cell RNA sequencing of microglia, pvMΦ, their proposed precursors, the monocytes and peritoneal macrophages (ptMΦ) (Fig. 1d and Supplementary Figs. 1 and 2). Individual RNA molecules were counted using unique molecular identifiers (UMIs) as described previously¹⁸, which greatly reduces PCR amplification bias. Dimensionality reduction using *t*-distributed stochastic network embedding (t-SNE)¹⁹ revealed that pvMΦ and microglia were

transcriptionally closely related, whereas monocytes and ptMΦ had a distinct RNA profile. All myeloid populations expressed the genes encoding the markers CX₃CR1, CSF-1R and Iba-1 (Fig. 1e), but pvMΦ were distinguishable from microglia on the basis of their expression of *Mrc1* (encoding CD206) and *Cd36* (Fig. 1f). Microglia expressed higher levels of *P2ry12* and *Hexb* than pvMΦ (Fig. 1g), whereas monocytes exclusively expressed *Cdc20* (Supplementary Fig. 1). Notably, *Ptprc* (encoding CD45) mRNA transcript expression was higher in pvMΦ than in microglia (Fig. 1e), which could be confirmed at the protein level for all non-parenchymal macrophages *in situ*, but not for microglia (Fig. 1h). Furthermore, the detection of CD206 protein on *Cx3cr1*^{GFP/WT} pvMΦ located in the perivascular space (laminin⁺), but not on parenchymal microglia, is consistent with our findings on RNA level (Fig. 1i). Flow cytometry-based separation of CD45^{hi}CD11b⁺CD206⁺ pvMΦ and CD45^{lo}CD11b⁺CD206⁻ microglia from mouse cortex that was free of meninges and choroid plexus enabled us to confirm the results obtained from the single-cell RNA sequencing on the protein level in a quantitative manner (Fig. 1j,k and Supplementary Fig. 2).

Taken together, these data show a close transcriptional relationship between non-parenchymal macrophages such as pvMΦ and microglia, albeit with some cell type-specific differences.

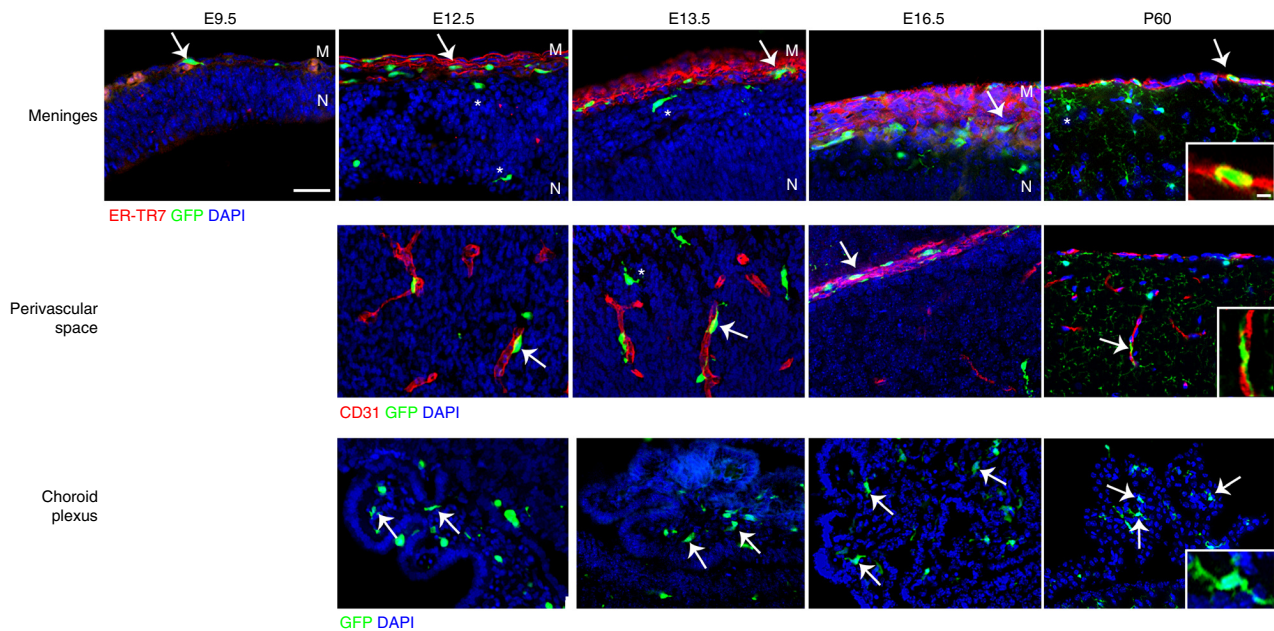


Figure 2 Development of CNS macrophages. Macrophage development in *Cx3cr1*^{GFP/WT} mice. Sagittal brain sections from E9.5 to adulthood (P60) of *Cx3cr1*^{GFP/WT} mice depicting subdural meningeal fibroblasts (ER-TR7, red), endothelial cells (CD31, red) and myeloid cells (GFP, green) together with nuclear staining (DAPI, blue). As early as E9.5, elongated GFP⁺ macrophages first appeared in the meninges (arrow) adjacent to the neuroectodermal border. CX₃CR1-GFP⁺ macrophages started seeding the neuroectoderm at E9.5 to become parenchymal microglia (asterisk). GFP⁺ pvMΦ and cpMΦ were clearly detectable starting from E12.5 onwards (arrows). Scale bar, 25 μm (overview) and 1 μm (inset). Data are representative of two independent experiments with three mice per time point.

Prenatal origin of CNS macrophages

The current concept that macrophages at CNS borders are derived from blood-borne myeloid cells during adulthood largely depends on previous work on BM chimeras using irradiation of the recipient^{20,21}, a finding that we were able to confirm by transplanting BM from *Acta1*-GFP mice, which ubiquitously express GFP in all cells of the body, into irradiated hosts, which led to a vigorous engraftment of donor-derived GFP⁺Iba-1⁺ macrophages in the subdural meninges, perivascular spaces and choroid plexus, whereas microglial exchange was limited (Supplementary Fig. 3).

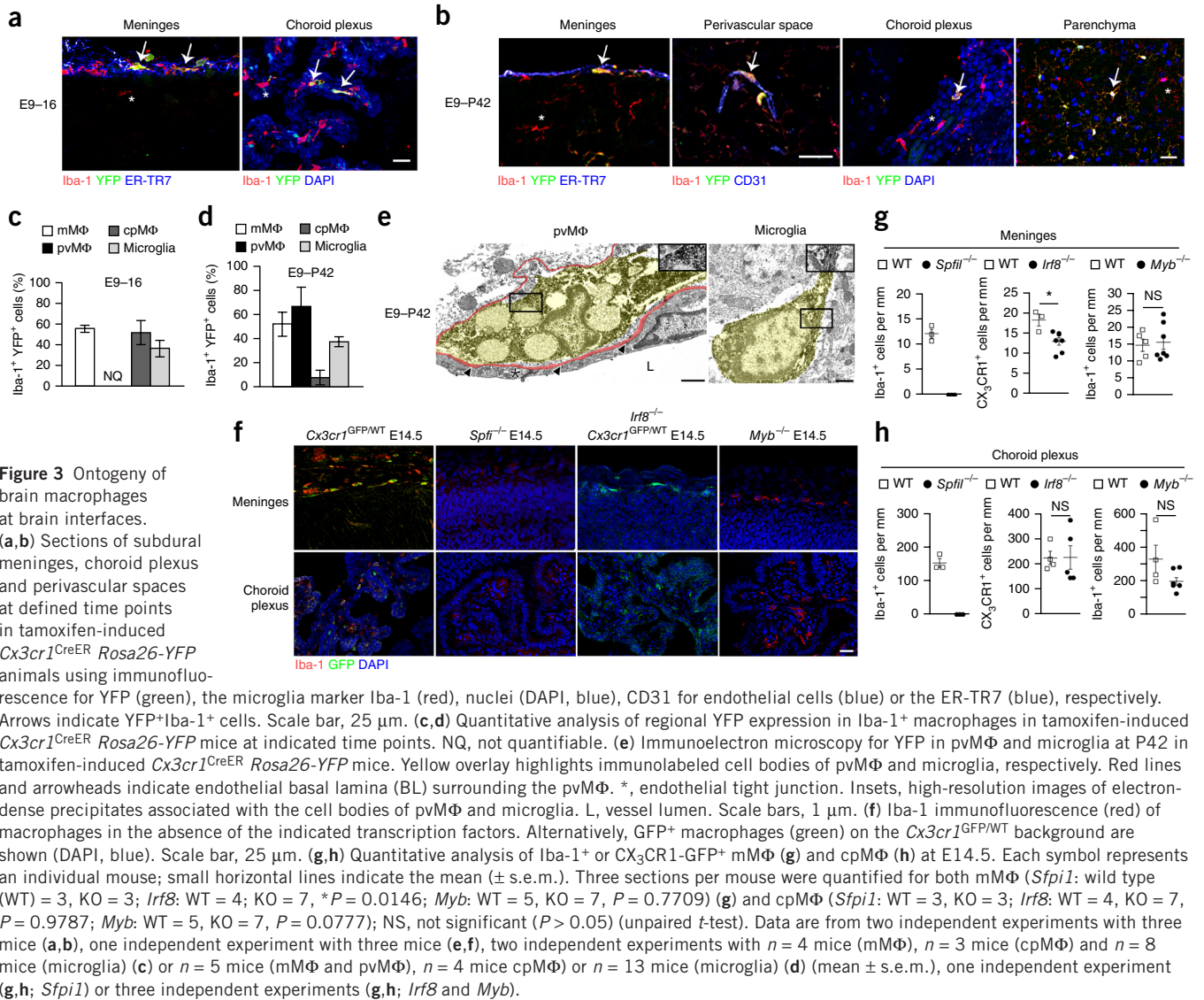
However, in several organs, resident macrophages arise from embryonic precursors in the yolk sac or fetal liver that seed the tissue before birth^{5-7,22-24}. Consistent with these findings, we observed *Cx3cr1*^{GFP/WT} macrophages in the subdural meninges at embryonic day 9.5 (E9.5) and shortly thereafter in the choroid plexus and the perivascular spaces (Fig. 2), suggesting prenatal seeding of tissue macrophages in these compartments. To test whether embryonic progenitors indeed contribute to the pool of CNS macrophages, we adapted a *Cx3cr1*^{CreER} mouse system that allows fate-mapping studies by tamoxifen-induced recombination in *Cx3cr1*-expressing cells at defined time points^{25,26}. Timed pregnancies were set up to generate *Cx3cr1*^{CreER} *Rosa26-YFP* embryos that undergo recombination and subsequently express YFP under the control of the *Rosa26* promoter after a single intraperitoneal injection of tamoxifen in pregnant wild-type mice at E9.0 to pulse *Cx3cr1*-expressing progenitor cells in the embryo (Supplementary Fig. 3a). This approach induced irreversible expression of YFP in *Cx3cr1*-expressing cells and their progeny. At E16.0, 55.4 ± 3.3% Iba-1⁺ mMΦ, 51.3 ± 11.5% Iba-1⁺ cpMΦ and 36.2 ± 7.5% Iba-1⁺ microglia expressed YFP, indicating robust labeling efficiency of the CX₃CR1⁺ progenitors (Fig. 3a,b). Although YFP⁺ pvMΦ could be recognized at this embryonic stage, they were too sparse to allow a reliable quantification in *Cx3cr1*^{CreER} *Rosa26-YFP* embryos. Considering that microglia are

entirely of prenatal origin (for example, from the yolk sac^{3,5}), we could also assume that pvMΦ, mMΦ and cpMΦ have their major source in embryonic hematopoietic sources such as the yolk sac. However, *Cx3cr1*-expressing myeloid progenitor cells are also found in the fetal liver²², which was why CNS macrophages could be derived from this prenatal source as well.

Not only microglia, but also pvMΦ and mMΦ, retained the YFP label in 6-week-old mice, demonstrating that embryonic labeling persisted into adulthood (Fig. 3c,d). In contrast, cpMΦ lost their YFP label over time, indicating that embryo-derived cells were replaced in the choroid plexus. Expression of YFP in pvMΦ in the perivascular space was confirmed by immunoelectron microscopy (Fig. 3e). Several transcription factors have been shown to be important for lineage commitment in myeloid cells^{27,28}. To determine which transcription factors are required for non-parenchymal CNS MΦ development, we investigated the presence of CNS macrophages in mutants lacking *Sfp1* (encoding PU.1), *Irf8*, *Myb* and *Batf3* (Fig. 3f-h and Supplementary Fig. 4a). Mice lacking PU.1 were devoid of any pvMΦ, mMΦ and cpMΦ. Notably, we found a reduction in the numbers of mMΦ, but not cpMΦ, in *Irf8*^{-/-} mice, whereas the absence of the master transcription factor for stem cell development in the BM, MYB, did not impair mMΦ and cpMΦ development, similar to its redundant role for yolk sac-derived macrophages such as microglia⁶. *Batf3* deficiency did not impair the development of any of the investigated macrophage populations. In summary, our data suggest mMΦ, pvMΦ, cpMΦ and microglia are all of prenatal origin, either from the yolk sac and/or the fetal liver, and largely depend on similar transcription factors for proper development.

Maintenance of pvMΦ, mMΦ and cpMΦ in adulthood

Once established in the CNS, microglia persist throughout the entire life of the organism without any substantial input from circulating blood cells as a result of their longevity and their capacity for



self-renewal^{13,29}. Thus, we sought to use this unique feature of microglia to compare their exchange kinetics with mMΦ, pvMΦ, cpMΦ and blood cells, such as monocytes. We treated adult *Cx3cr1^{CreER} Rosa26-YFP* mice^{25,26} with tamoxifen and determined mMΦ, pvMΦ and cpMΦ labeling at several time points after application (Supplementary Fig. 3b). Flow cytometry revealed long-term labeling of YFP⁺CD45^{hi}CD11b⁺ non-parenchymal macrophages, even 30 weeks after tamoxifen treatment (Fig. 4a). Histological examination confirmed the flow cytometry data and revealed a high percentage of Iba-1-labeled mMΦ, pvMΦ and cpMΦ that coexpressed YFP (Fig. 4b). Quantitative examination on histological slices showed constant high expression of the reporter gene in mMΦ and pvMΦ, comparable to what we observed in microglia (Fig. 3d). These data indicate that mMΦ and pvMΦ are stable populations that do not undergo substantial exchange with blood cells over 46 weeks. In contrast, YFP-labeling progressively dropped in Iba-1⁺ cpMΦ, suggesting a slow continuous exchange with blood cells. As a result of their transient nature *Cx3cr1*-targeted Ly6C^{lo} monocytes in the blood lost their YFP reporter very rapidly and were quickly replaced by the non-targeted progeny^{25,26,30}. Confocal analysis further confirmed the long-term persistence of pvMΦ in perivascular

spaces of cerebral vessels (limited by laminin⁺ basement membranes) at 8 weeks after tamoxifen treatment (Fig. 4c,d). At this time point, microglia were still labeled, but blood monocytes were not (Fig. 4e). Notably, we detected YFP-expressing mMΦ and cpMΦ by immunoelectron microscopy 30 weeks after recombination (Fig. 4f). Labeled cpMΦ were found in close proximity to the microvilli of the choroid plexus epithelium, indicating that these cells represent Kolmer's epiplexus cells.

To further analyze whether the presence of these long-lived myeloid cells in distinct CNS microenvironments shapes their dynamic behavior, we imaged fluorescently labeled mMΦ, pvMΦ and microglia of living *Cx3cr1^{CreER} Rosa26-Tomato* mice at 8 weeks after tamoxifen treatment by confocal and *in vivo* two-photon (2p) microscopy. We found Tomato⁺ cells in the subdural meninges, perivascular space and choroid plexus that expressed the markers F4/80 and CD206, indicating their macrophage nature (Fig. 5a and Supplementary Fig. 4b). 2p time-lapse imaging revealed that mMΦ, pvMΦ and microglia, which are all embryo derived, can be differentiated *in vivo* not only on the basis of their anatomical location, but also of their characteristic morphology and distinct dynamic behavior (Fig. 5b-e and Supplementary Videos 1 and 2). Consistent with previous

reports^{31,32}, microglial cells showed a ramified morphology with highly dynamic processes and a rather stationary cell body. In contrast, mMΦ often presented with a more amoeboid morphology, and about a third of these cells (62 of 172 cells) moved over time (Fig. 5e,f). These cell types could be further differentiated from pvMΦ, which followed the blood vessel outline and rarely displaced their cell body

(5 of 44 cells), but constantly extended and retracted their protrusions along the blood vessel wall.

To evaluate a possible contribution of blood cells to the pool of macrophages at CNS boundaries under homeostatic conditions, we needed a method for tracking circulating cells without affecting the CNS environment or resident cells. Thus, we induced peripheral blood

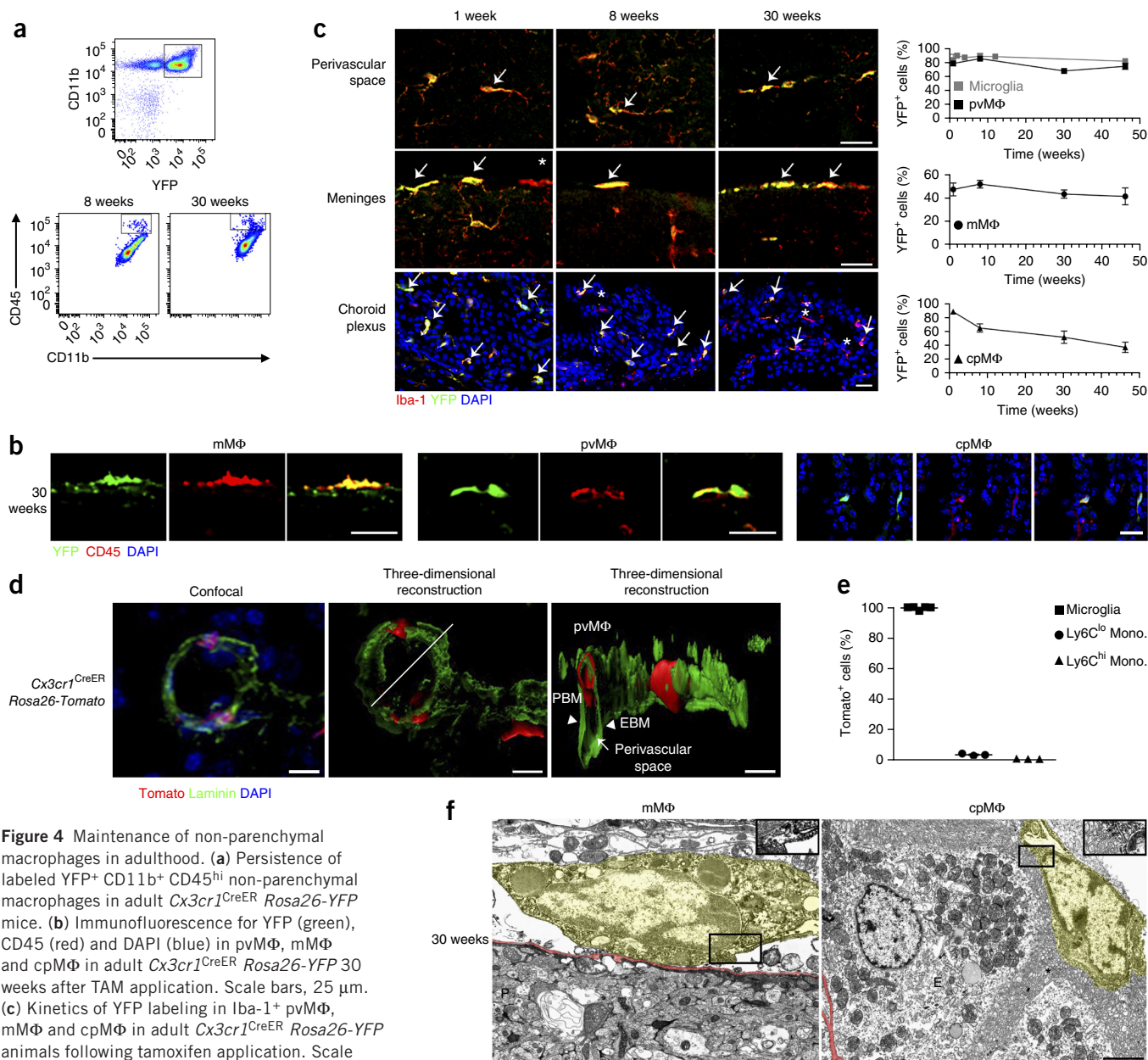


Figure 4 Maintenance of non-parenchymal macrophages in adulthood. **(a)** Persistence of labeled YFP⁺ CD11b⁺ CD45^{hi} non-parenchymal macrophages in adult *Cx3cr1^{CreER} Rosa26-YFP* mice. **(b)** Immunofluorescence for YFP (green), CD45 (red) and DAPI (blue) in pvMΦ, mMΦ and cpMΦ in adult *Cx3cr1^{CreER} Rosa26-YFP* 30 weeks after TAM application. Scale bars, 25 μm.

(c) Kinetics of YFP labeling in Iba-1⁺ pvMΦ, mMΦ and cpMΦ in adult *Cx3cr1^{CreER} Rosa26-YFP* animals following tamoxifen application. Scale bars, 25 μm. *, single-positive cells; arrows indicate double-positive cells.

(d) Localization of Tomato⁺ pvMΦ (red) in the perivascular space using confocal microscopy (left) and three-dimensional reconstruction (middle, right) in adult *Cx3cr1^{CreER} Rosa26-Tomato* animals 8 weeks after tamoxifen injection. Laminin (green) is used to indicate the parenchymal and endothelial basement membranes and nuclei are counterstained with DAPI (blue). Line indicates the cross section of the three-dimensional reconstruction (right). Arrowheads and arrow point indicate structures. Scale bars, 10 μm (middle) and 5 μm (right).

(e) Quantification of Tomato labeling 8 weeks after tamoxifen application. Each symbol represents an individual mouse; small horizontal lines indicate the mean (± s.e.m.). **(f)** Immunoelectron microscopy for YFP in *Cx3cr1^{CreER} Rosa26-YFP* mice 30 weeks after TAM application reveals positively labeled mMΦ and cpMΦ. Yellow overlay marks immunolabeled cell bodies of mMΦ and Kolmer's epilexus cell (cpMΦ). *, microvilli of the choroid plexus epithelium. Red lines indicate the basal lamina (BL). Insets, high-resolution pictures of electron-dense precipitates associated with the cell bodies of mMΦ and cpMΦ. E, epithelium; P, parenchyma. Scale bars, 1 μm (left) and 2 μm (right). Data are from two independent experiments with five mice (**a**), two independent experiments with three mice (**b**), one independent experiment with three mice (**c**, left), two independent experiments (**c**, right; mean ± s.e.m. of $n = 18$ mice (microglia), $n = 15$ mice (pvMΦ), $n = 13$ mice (mMΦ) or $n = 14$ mice (cpMΦ)), three independent experiments with three mice (**d**), two independent experiments (**e**; $n = 5$ mice for microglia; $n = 3$ for Ly6C^{lo} and Ly6C^{hi} monocytes) or one independent experiment with two mice (**f**).

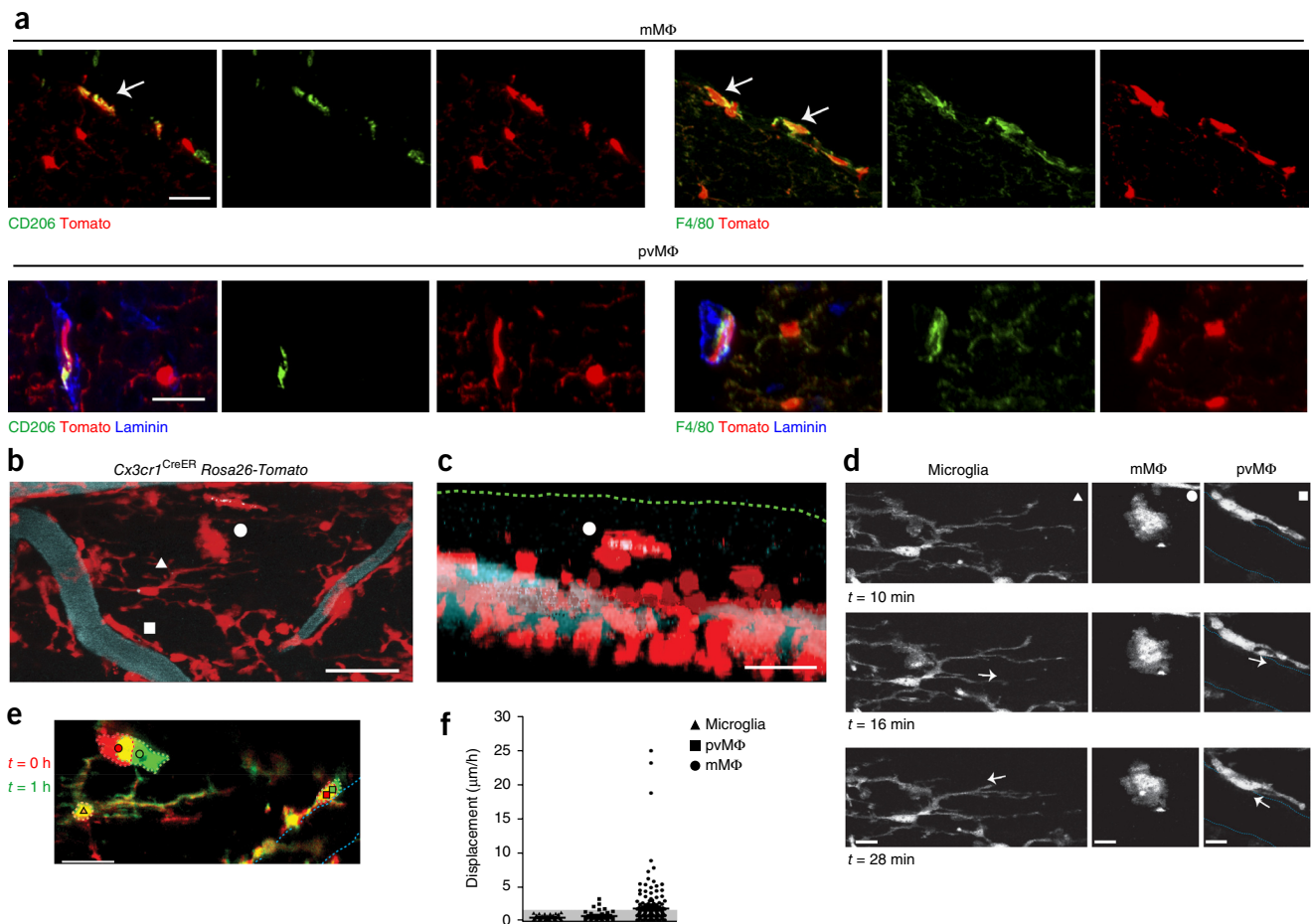


Figure 5 *In vivo* dynamics of CNS macrophages. (a) Immunofluorescence microscopy of Tomato⁺ cells in subdural meninges and perivascular space (laminin⁺ BM in blue) of *Cx3cr1^{CreER} Rosa26-Tomato* mice are labeled for CD206 and F4/80. Scale bars, 25 μm (mMΦ) or 10 μm (pvMΦ). (b) Confocal microscopy of *Cx3cr1^{CreER} Rosa26-Tomato* mice (tomato, red) injected with dextran-AF647 (blue) for the vasculature. pvMΦ, square; mMΦ, circle; microglia, triangle. Scale bar, 25 μm. (c) Z-projection of **b** showing localization of the mMΦ. Green dotted line represents upper limit of the dura membrane. Scale bar, 25 μm. (d) *In vivo* 2p time lapse of the myeloid cells marked in **b** showing the dynamic behavior of microglia cell processes (left), a subdural mMΦ (middle) and a pvMΦ (right) in *Cx3cr1^{CreER} Rosa26-Tomato* mice (tomato, red). White arrows indicate direction of dynamic changes. Scale bars, 2.4 μm (left), 1.0 μm (middle) or 1.2 μm (right). (e) Overlay of two 2p image projections of the dorsal spinal surface of a *Cx3cr1^{CreER} Rosa26-Tomato* mouse at *t* = 0 h (red) and *t* = 1 h (green) showing the displacement of cell somata over time. Dashed lines indicate cell-body contours at 0 h (red) and 1 h (green); cyan dotted line outlines the vasculature. Scale bar, 20 μm. (f) Quantification of *in vivo* cell-body displacement of microglia, pvMΦ and mMΦ of *Cx3cr1^{CreER} Rosa26-Tomato* mice at 8 weeks after TAM injection. Each symbol represents an individual mouse; small horizontal lines indicate the mean gray shaded area represents the average + 3 s.d. of the cell displacement of microglia cells. Data are from two independent experiments with five mice (a), one independent experiment with two mice (b,c), two independent experiments with five mice (d,e) or two independent experiments with five mice from (f; *n* = 41 microglial cells, *n* = 44 pvMΦ and *n* = 172 mMΦ).

chimerism by surgically joining two syngeneic mice, one of which ubiquitously expressed GFP (*Acta1-GFP*). These parabiotic mice established a rich anastomotic circulation, which quickly led to efficient blood chimerism in peripheral Ly6C^{hi} and Ly6C^{lo} monocytes (Fig. 6a)³³. However, there was no detectable circulatory exchange of mMΦ and pvMΦ after 5 months of parabiosis, whereas donor-derived blood cells contributed to the cpMΦ population (Fig. 6a). Furthermore, low gene recombination of mMΦ and pvMΦ in *Flt3^{Cre} Rosa26-YFP* animals suggested that their development occurred largely independently of Flt3⁺ multipotent hematopoietic precursors in the BM compared with the high percentage of YFP⁺ myeloid cells in the circulation (Fig. 6b). Again, only cpMΦ displayed a higher recombination of this gene, suggesting a role for hematopoietic stem cells in the development of cpMΦ. Furthermore, we found that neither Ly6C^{hi} nor Ly6C^{lo} monocytes were essential for mMΦ and pvMΦ development, as mice lacking *Ccr2* or *Nr4a1* presented normal proportions of these macrophages

subsets (Fig. 6c). Only cpMΦ were reduced in *Ccr2*-deficient mice, indicating that Ly6C^{hi} monocytes contribute to their homeostasis. In sum, these data clearly indicate that non-parenchymal MΦ, such as mMΦ and pvMΦ, share their longevity with microglia without any input from blood monocytes (Supplementary Fig. 5). Only cpMΦ are exceptional, which, because of their dual origin, have a partial input from the circulation and a shorter turnover.

DISCUSSION

Our results describe the molecular signatures of tissue macrophages at CNS boundaries, their developmental pathways and the key mechanisms that ensure their homeostasis. By using large-scale single-cell RNA sequencing, we were able to dissect the individual transcriptional profiles of cortical pvMΦ and parenchymal myeloid cells (microglia) in the CNS and found a close relationship between these cells that was not shared by circulating monocytes or ptMΦ. Our unbiased

high-throughput methodology allowed us to define extensive functional specialization between cell classes¹⁸. In fact, we found that the marker *Mrc1* was enriched in macrophages at CNS interfaces, whereas *P2ry12* was expressed only by microglia, which confirms previous

data that used expression profiling of several thousands of cells in the CNS^{34,35}. However, our finding that mM Φ , pvM Φ and cpM Φ have only limited relation to circulating myeloid cells represents a major conceptual change in the field. Since the 1980s, it has been assumed,

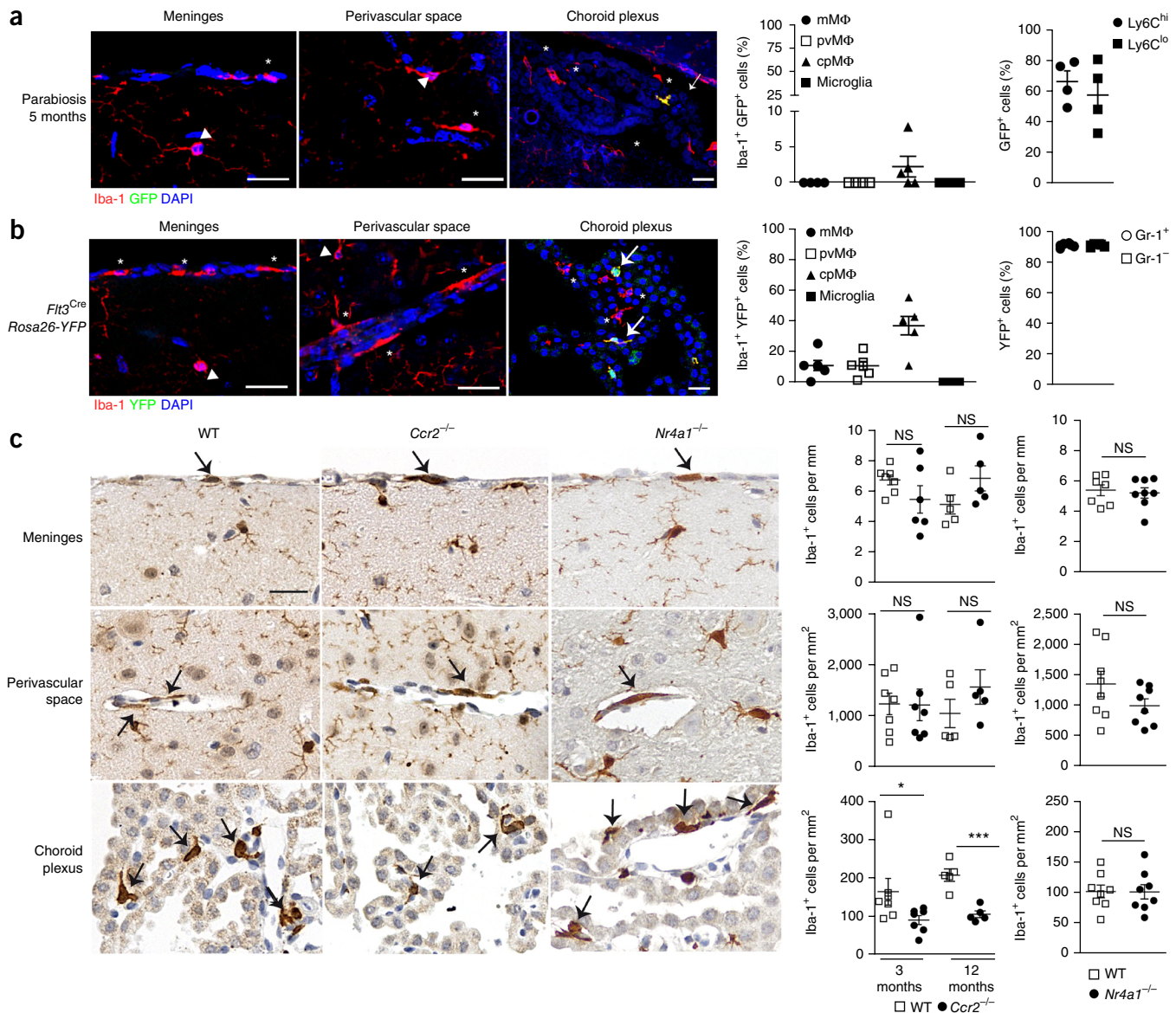


Figure 6 Turnover of CNS macrophages. (a) Immunofluorescence microscopy (left) showing negligible exchange of cpM Φ and no contribution to pvM Φ , mM Φ and microglia in a wild-type parabiont after 5 months of parabiosis with an *Acta1*-GFP mouse. *, single-positive cells; arrows, double-positive cells; arrowheads, microglia. Scale bars, 25 μ m. Right, quantification of results at left (left plot), and blood chimerism for (CD45⁺ CD11b⁺ CD115⁺) Ly6C^{hi} and Ly6C^{lo} monocytes (far right). (b) Immunofluorescence microscopy (left) showing little *Flt3* expression as a marker of definitive hematopoiesis in pvM Φ , mM Φ and cpM Φ in adult *Flt3^{Cre} Rosa26-YFP* mice. Scale bars, 25 μ m. Right, quantification of results at left (left plot), and recombination efficiency of circulating CD11b⁺Gr-1⁺CD3⁻CD19⁻ inflammatory monocytes (Gr-1⁺) and CD11b⁺Gr-1⁻CD3⁻CD19⁻ resident monocytes (Gr-1⁻), assessed by flow cytometry. (c) Iba-1 immunohistochemistry (brown) showing the localization and presence of pvM Φ , mM Φ and cpM Φ in adult wild-type (WT), *Ccr2*^{-/-} and *Nr4a1*^{-/-} mice (left), and quantification of results at left (right). *Ccr2*^{-/-} mice (meninges: 3 months WT = 7 mice, 3 months KO = 6, unpaired *t* test *P* = 0.1795; 12 months WT = 5, 12 months KO = 5, unpaired *t* test *P* = 0.1354; perivascular space: 3 months WT = 7 mice, 3 months KO = 7, unpaired *t* test *P* = 0.9613; 12 months WT = 5, 12 months KO = 5, Mann-Whitney test *P* = 0.4206; choroid plexus: 3 months WT = 7 mice, 3 months KO = 7, Mann-Whitney test **P* = 0.0379; 12 months WT = 5, 12 months KO = 5, unpaired *t* test ****P* = 0.0005); *Nr4a1*^{-/-} mice (meninges: WT = 7 mice, KO = 8, unpaired *t* test *P* = 0.7282; perivascular space: WT = 8 mice, KO = 8, unpaired *t* test *P* = 0.1566; choroid plexus: WT = 8 mice, KO = 8, unpaired *t* test *P* = 0.9658). NS, not significant (*P* > 0.05). Each symbol (a–c, right) represents an individual mouse; small horizontal lines indicate the mean (\pm s.e.m.) Data are from one independent experiment with three mice (a, left images), four mice (a, far right) or *n* = 4 mice (mM Φ , pvM Φ and microglia) or *n* = 5 mice (cpM Φ) with at least three tissue sections (a, left plot), two independent experiments with three mice (b, left images), three mice (b, far right) or *n* = 6 mice per cell population (b, left plot) or two independent experiments with five mice per genotype (c, left), three mice (wild-type and *Ccr2*^{-/-}) or three (wild-type and *Nr4a1*^{-/-}) independent experiments with at least three tissue sections (c, right).

based on BM chimera data using whole-body irradiation, that macrophages at CNS interfaces are blood derived⁹. The involvement of the CNS during the irradiation procedure clearly leads to substantial local priming with concomitant induction of myelo-attracting and myelo-promoting factors and damage of the BBB^{7,13–15}. Consequently, all previous studies on mMΦ, pvMΦ and cpMΦ using these techniques to establish BM chimeras have to be interpreted with caution.

Tissue macrophages arise from two distinct embryonic developmental programs: early yolk sac-derived erythromyeloid progenitors (EMPs) that give rise to macrophages without monocyte intermediates and fetal monocytes that derive from MYB⁺ EMPs generated in the yolk sac^{7,22,36}. These pathways contribute differentially to macrophage development in several tissues, including the aorta, brain, skin, heart, liver and lung^{7,22,24,37–39}. Consistent with these findings, we found *Cx3cr1*-GFP⁺ mMΦ, pvMΦ and cpMΦ during early embryogenesis, and fate-mapping approaches confirmed the persistence of embryo-derived CNS macrophages in embryonic, as well as in adult, mice. Development and homeostasis of CNS macrophages is not uniform. Similar to microglia, the maintenance of mMΦ and pvMΦ did not depend on circulating monocytes, and non-parenchymal CNS macrophages persisted over a very long period of time.

This is in contrast with cpMΦ, which show features of relative transience (compared with other CNS MΦ) and some replenishment by blood cells. A report conflicting with this interpretation suggests a different origin for all tissue macrophages, with the exception microglia, namely that they are derived from sources of definitive (fetal) hematopoiesis⁴⁰. Using our *Cx3cr1*^{CreER} *Rosa26-YFP* fate-mapping system that tracks distinct yolk sac cells, we were able to clearly show that, in contrast with this earlier report⁴⁰ and in agreement with another study²², several other tissues such as the subdural meninges, the cerebral perivascular space and the choroid plexus contain MΦ that are derived from early embryonic precursors and remain there until adulthood.

Flt3 is expressed only by definitive hematopoietic progenitors in the embryo and during adulthood⁴¹. It can therefore be used to distinguish yolk sac-derived versus BM-derived macrophages⁴². This approach helped us to define cpMΦ as a distinct population of CNS macrophages that is different from mMΦ, pvMΦ and microglia that only have a negligible input from *Flt3*-dependent definitive hematopoiesis. CpMΦ development from circulating monocytes was confirmed by our results from the parabiosis experiments and in *Ccr2*-deficient mice. In contrast, genetic labeling using the tamoxifen-inducible *Cx3cr1*^{CreER} *Rosa26-YFP* system revealed that mMΦ and pvMΦ remained markedly stable when compared between embryonic and adult animals, arguing against a substantial contribution of BM-derived monocytes to these macrophages population, which is in contrast with other tissue macrophage populations such as in the liver and gut²². However, the small portion of *Flt3*-dependent YFP-labeled mMΦ and pvMΦ could also indicate another cellular origin of mMΦ and pvMΦ except from the yolk sac, namely from yolk sac-derived EMPs or monocytes that seed the fetal liver. Using our *Cx3cr1*^{CreER} *Rosa26-YFP* fate mapping system, we could not distinguish between these different embryonic sources.

Neurological diseases in which the choroid plexus is crucially involved as one of the interfaces between periphery and CNS are abundant⁴³. Several lines of evidence suggest a fundamental involvement of the choroid plexus in the development and progression of multiple sclerosis (MS) and its animal model EAE. First, choroid plexus inflammation with immune cell activation and infiltration has been described preceding parenchymal inflammation and clinical disease onset in humans and mice⁴⁴. Second, auto-aggressive

sentinel T cells are thought to enter the cerebrospinal fluid through the choroid plexus during incipient stages of MS and EAE, and then travel to the subarachnoid space, where they are reactivated by local antigen-presenting cells (APCs) presenting cognate antigen⁴⁵. These findings all argue for the dual role of the choroid plexus as an immune cell-modulatory site, as well as an entry gate for peripheral immune cells to the CNS during neuroinflammation.

Strategically positioned at the CNS barriers, mMΦ, pvMΦ and cpMΦ might modulate immune cell entry and phenotype. The myeloid cells in the CNS-adjointing tissues have been implicated in various immunopathological processes, including antigen presentation to circulating lymphocytes^{46–48}. As presumed guardians of tissue homeostasis, the CNS-surrounding myeloid cell network appears to be crucially involved in the development, progression and resolution of neuroinflammatory, neurodegenerative and neurooncological diseases. Our results will help to unravel mMΦ, pvMΦ and cpMΦ function *in vivo* in more detail and to identify new means to manipulate these cells for the treatment of neural diseases.

METHODS

Methods and any associated references are available in the [online version of the paper](#).

Note: Any Supplementary Information and Source Data files are available in the online version of the paper.

ACKNOWLEDGMENTS

We thank M. Oberle, M. Ditter and T. el Gaz for excellent technical assistance and T. Leng Tay for critical reading of the manuscript. Supported by the DFG (SFB 992, SFB 1160, PR 577/8-1, Reinhart Koselleck Grant for M.P.; SFB 1160, ZE872/3-1 for R.Z.; and FOR1336 for J.P., I.B., M.P. and S.J.), the Fritz-Thyssen Foundation (M.P.), the European Union's Seventh Framework Program FP7 under Grant agreement 607962 (nEUROinflammation for M.P.), the Gemeinnützige Hertie Foundation (GHST for M.P.), the Sobek Foundation (M.P.) and the BMBF-funded Competence Network on Multiple Sclerosis (KKNMS for M.P. and M. Kerschensteiner).

AUTHOR CONTRIBUTIONS

T.G., P.W., M.J.C.J., F.P., N.H., K.F., O.S., K.K., L.A., M. Krueger, G.L. and H.H. conducted the experiments and analyzed the data. R.Z., S.E., F.G., J.P., F.M.V.R., I.B., S.L., M. Kerschensteiner and S.J. analyzed the data, contributed to the *in vivo* studies and provided mice or reagents. T.G. and M.P. supervised the project and wrote the manuscript.

COMPETING FINANCIAL INTERESTS

The authors declare no competing financial interests.

Reprints and permissions information is available online at <http://www.nature.com/reprints/index.html>.

- Ransohoff, R.M. & Cardona, A.E. The myeloid cells of the central nervous system parenchyma. *Nature* **468**, 253–262 (2010).
- Prinz, M., Priller, J., Sisodia, S.S. & Ransohoff, R.M. Heterogeneity of CNS myeloid cells and their roles in neurodegeneration. *Nat. Neurosci.* **14**, 1227–1235 (2011).
- Prinz, M. & Priller, J. Microglia and brain macrophages in the molecular age: from origin to neuropsychiatric disease. *Nat. Rev. Neurosci.* **15**, 300–312 (2014).
- Alliot, F., Godin, I. & Pessac, B. Microglia derive from progenitors, originating from the yolk sac, and which proliferate in the brain. *Brain Res. Dev. Brain Res.* **117**, 145–152 (1999).
- Ginhoux, F. *et al.* Fate-mapping analysis reveals that adult microglia derive from primitive macrophages. *Science* **330**, 841–845 (2010).
- Schulz, C. *et al.* A lineage of myeloid cells independent of Myb and hematopoietic stem cells. *Science* **336**, 86–90 (2012).
- Kierdorf, K. *et al.* Microglia emerge from erythromyeloid precursors via Pu.1- and Irf8-dependent pathways. *Nat. Neurosci.* **16**, 273–280 (2013).
- Aguzzi, A., Barres, B.A. & Bennett, M.L. Microglia: scapegoat, saboteur, or something else? *Science* **339**, 156–161 (2013).
- Hickey, W.F. & Kimura, H. Perivascular microglial cells of the CNS are bone marrow-derived and present antigen *in vivo*. *Science* **239**, 290–292 (1988).
- Hickey, W.F., Vass, K. & Lassmann, H. Bone marrow-derived elements in the central nervous system: an immunohistochemical and ultrastructural survey of rat chimeras. *J. Neuropathol. Exp. Neurol.* **51**, 246–256 (1992).

11. Yang, Y. *et al.* Perivascular, but not parenchymal, cerebral engraftment of donor cells after non-myeloablative bone marrow transplantation. *Exp. Mol. Pathol.* **95**, 7–17 (2013).
12. Barr, C.M., Manning, J., Lewis, C.A., Rossi, F.M. & Krieger, C. Submyeloablative conditioning with busulfan permits bone marrow-derived cell accumulation in a murine model of Alzheimer's disease. *Neurosci. Lett.* **588**, 196–201 (2015).
13. Mildner, A. *et al.* Microglia in the adult brain arise from Ly-6ChiCCR2+ monocytes only under defined host conditions. *Nat. Neurosci.* **10**, 1544–1553 (2007).
14. Mildner, A. *et al.* Distinct and non-redundant roles of microglia and myeloid subsets in mouse models of Alzheimer's disease. *J. Neurosci.* **31**, 11159–11171 (2011).
15. Kierdorf, K., Katzmarski, N., Haas, C.A. & Prinz, M. Bone marrow cell recruitment to the brain in the absence of irradiation or parabiosis bias. *PLoS One* **8**, e58544 (2013).
16. Galea, I. *et al.* Mannose receptor expression specifically reveals perivascular macrophages in normal, injured and diseased mouse brain. *Glia* **49**, 375–384 (2005).
17. Kim, J.V., Kang, S.S., Dustin, M.L. & McGavern, D.B. Myelomonocytic cell recruitment causes fatal CNS vascular injury during acute viral meningitis. *Nature* **457**, 191–195 (2009).
18. Zeisel, A. *et al.* Brain structure. Cell types in the mouse cortex and hippocampus revealed by single-cell RNA-seq. *Science* **347**, 1138–1142 (2015).
19. Jamieson, A.R. *et al.* Exploring nonlinear feature space dimension reduction and data representation in breast Cdx with Laplacian eigenmaps and t-SNE. *Med. Phys.* **37**, 339–351 (2010).
20. Bechmann, I. *et al.* Turnover of rat brain perivascular cells. *Exp. Neurol.* **168**, 242–249 (2001).
21. Priller, J. *et al.* Targeting gene-modified hematopoietic cells to the central nervous system: use of green fluorescent protein uncovers microglial engraftment. *Nat. Med.* **7**, 1356–1361 (2001).
22. Gomez Perdiguero, E. *et al.* Tissue-resident macrophages originate from yolk-sac-derived erythro-myeloid progenitors. *Nature* **518**, 547–551 (2015).
23. Molawi, K. *et al.* Progressive replacement of embryo-derived cardiac macrophages with age. *J. Exp. Med.* **211**, 2151–2158 (2014).
24. Ensan, S. *et al.* Self-renewing resident arterial macrophages arise from embryonic CX3CR1 precursors and circulating monocytes immediately after birth. *Nat. Immunol.* **17**, 159–168 (2015).
25. Yona, S. *et al.* Fate mapping reveals origins and dynamics of monocytes and tissue macrophages under homeostasis. *Immunity* **38**, 79–91 (2013).
26. Goldmann, T. *et al.* A new type of microglia gene targeting shows TAK1 to be pivotal in CNS autoimmune inflammation. *Nat. Neurosci.* **16**, 1618–1626 (2013).
27. Rosenbauer, F. & Tenen, D.G. Transcription factors in myeloid development: balancing differentiation with transformation. *Nat. Rev. Immunol.* **7**, 105–117 (2007).
28. Geissmann, F. *et al.* Development of monocytes, macrophages, and dendritic cells. *Science* **327**, 656–661 (2010).
29. Ajami, B., Bennett, J.L., Krieger, C., Tetzlaff, W. & Rossi, F.M. Local self-renewal can sustain CNS microglia maintenance and function throughout adult life. *Nat. Neurosci.* **10**, 1538–1543 (2007).
30. Wieghofer, P., Knobeloch, K.P. & Prinz, M. Genetic targeting of microglia. *Glia* **63**, 1–22 (2015).
31. Nimmerjahn, A., Kirchhoff, F. & Helmchen, F. Resting microglial cells are highly dynamic surveillants of brain parenchyma *in vivo*. *Science* **308**, 1314–1318 (2005).
32. Davalos, D. *et al.* ATP mediates rapid microglial response to local brain injury *in vivo*. *Nat. Neurosci.* **8**, 752–758 (2005).
33. Ajami, B., Bennett, J.L., Krieger, C., McNagny, K.M. & Rossi, F.M. Infiltrating monocytes trigger EAE progression, but do not contribute to the resident microglia pool. *Nat. Neurosci.* **14**, 1142–1149 (2011).
34. Butovsky, O. *et al.* Identification of a unique TGF- β -dependent molecular and functional signature in microglia. *Nat. Neurosci.* **17**, 131–143 (2014).
35. Hickman, S.E. *et al.* The microglial sensome revealed by direct RNA sequencing. *Nat. Neurosci.* **16**, 1896–1905 (2013).
36. Ginhoux, F. & Jung, S. Monocytes and macrophages: developmental pathways and tissue homeostasis. *Nat. Rev. Immunol.* **14**, 392–404 (2014).
37. Chorro, L. *et al.* Langerhans cell (LC) proliferation mediates neonatal development, homeostasis, and inflammation-associated expansion of the epidermal LC network. *J. Exp. Med.* **206**, 3089–3100 (2009).
38. Guillemin, M. *et al.* Alveolar macrophages develop from fetal monocytes that differentiate into long-lived cells in the first week of life via GM-CSF. *J. Exp. Med.* **210**, 1977–1992 (2013).
39. Epelman, S. *et al.* Embryonic and adult-derived resident cardiac macrophages are maintained through distinct mechanisms at steady state and during inflammation. *Immunity* **40**, 91–104 (2014).
40. Sheng, J., Ruedl, C. & Karjalainen, K. Most tissue-resident macrophages except microglia are derived from fetal hematopoietic stem cells. *Immunity* **43**, 382–393 (2015).
41. Adolfsson, J. *et al.* Upregulation of Flt3 expression within the bone marrow Lin(–)Sca1(+)-kit(+) stem cell compartment is accompanied by loss of self-renewal capacity. *Immunity* **15**, 659–669 (2001).
42. Epelman, S., Lavine, K.J. & Randolph, G.J. Origin and functions of tissue macrophages. *Immunity* **41**, 21–35 (2014).
43. Kunis, G. *et al.* IFN- γ -dependent activation of the brain's choroid plexus for CNS immune surveillance and repair. *Brain* **136**, 3427–3440 (2013).
44. Engelhardt, B., Wolburg-Buchholz, K. & Wolburg, H. Involvement of the choroid plexus in central nervous system inflammation. *Microsc. Res. Tech.* **52**, 112–129 (2001).
45. Axtell, R.C. & Steinman, L. Gaining entry to an uninfamed brain. *Nat. Immunol.* **10**, 453–455 (2009).
46. Kivisäkk, P. *et al.* Localizing central nervous system immune surveillance: meningeal antigen-presenting cells activate T cells during experimental autoimmune encephalomyelitis. *Ann. Neurol.* **65**, 457–469 (2009).
47. Anandasabapathy, N. *et al.* Flt3L controls the development of radiosensitive dendritic cells in the meninges and choroid plexus of the steady-state mouse brain. *J. Exp. Med.* **208**, 1695–1705 (2011).
48. Brendecke, S.M. & Prinz, M. Do not judge a cell by its cover—diversity of CNS resident, adjoining and infiltrating myeloid cells in inflammation. *Semin. Immunopathol.* **37**, 591–605 (2015).

ONLINE METHODS

Mice. In this study, C57BL/6 and CD-1 mice were used as WT mice. All transgenic lines (*Acta1*-GFP mice, *Batf3*^{-/-}, *Ccr2*^{-/-}, *Cx3cr1*^{GFP/WT}, *Myb*^{-/-}, *Nr4a1*^{-/-}, *Irf8*^{-/-}*Cx3cr1*^{GFP/WT}, *Sfp1*^{-/-}, *Cx3cr1*^{CreER}, *Flt3*^{Cre}, *Rosa26-YFP* and *Rosa26-Tomato*) were bred on a C57BL/6 background in-house under pathogen-free conditions. *Cx3cr1*^{CreER} were crossed to either *Rosa26-YFP* or *Rosa26-Tomato* mice. *Flt3*^{Cre} were backcrossed to *Rosa26-YFP*. All animal experiments were approved by local administration (Regierungspräsidium Freiburg und München) and were performed in accordance to the respective national, federal and institutional regulations.

Tamoxifen treatment. For induction of the Cre recombinase in adult animals, 6–8-week-old *Cx3cr1*^{CreER} mice were treated twice with 4 mg tamoxifen (TAM, Sigma-Aldrich) solved in 200 μ l corn oil (Sigma), injected subcutaneously at two time points 48 h apart. For pulse-labeling experiments, the Cre recombinase was induced in *Cx3cr1*^{CreER} *Rosa26-YFP* embryos with 200 μ l of 20 mg ml⁻¹ TAM and 10 mg ml⁻¹ progesterone (Sigma) dissolved in corn oil by intraperitoneal injections into pregnant females at 9 d post coitum.

BM transplantation. 8-week-old WT recipient mice were lethally irradiated and reconstituted with 5×10^6 BM cells derived from femur and tibia of adult *Acta1*-GFP mice, injected into the tail vein of recipients. Mice received whole-body irradiation (11 Gy) 24 h before BM reconstitution with an RS 2000 Biologica x-Ray irradiator. After 4 weeks, reconstitution efficiency in the blood was assessed by flow cytometry and found to be higher > 90% in Ly6Ch^{hi} monocytes.

Parabiosis. Pairs of WT and *Acta1*-GFP mice were surgically connected for five months as previously described²⁹. Complete blood sharing was verified between 10 and 15 d after surgery and at the day of dissection by flow cytometry (see below). After transcatheter perfusion with phosphate-buffered saline (PBS), brains were fixed in 4% paraformaldehyde (PFA, wt/vol), dehydrated in 30% sucrose (wt/vol) and embedded in Tissue-Tek O.C.T. compound (Sakura Finetek Germany GmbH). Brains were further processed for immunofluorescence.

In vivo imaging and image processing. Animals were anesthetized with ketamine and xylazine (ketamine 87 mg per kg, xylazine 13 mg per kg), placed on a heating pad, and then tracheotomized and intubated. The dorsal spinal cord was surgically exposed as previously described⁴⁹ and the opening constantly superfused with artificial cerebrospinal fluid (aCSF). For the imaging session, the vertebral column was fixed using a spinal clamping device (Narishige STS-a) and the spinal opening surrounded by a 3% agarose well. Mice were injected intraperitoneally with 200 μ g of Dextran-AF647 (Life Technologies) to reveal the vasculature and the spinal cord was incubated with Nuclear-ID Blue dye (dilution 1:250, Enzo Life Sciences) for 15 min at 20–25 °C to reveal the meningeal surface as previously established⁵⁰. *In vivo* imaging was performed using confocal or 2p laser excitation on a Olympus FV1200 MPE setup equipped with a 25 \times /1.25 water immersion objective (Olympus) at 1,024 \times 1,024 pixel resolution. For confocal imaging, the Nuclear-ID Blue dye, tomato and Dextran-AF647 were sequentially excited using 405-nm, 568-nm and 647-nm lasers, respectively. For 2p time-lapse imaging of microglia/macrophage dynamics, the IR laser was tuned to 950 nm and fluorescence was collected using a standard green/red filter set (BA575-630). When needed, movement artifacts in the 2p movies were corrected using a registration plugin (Rigid body) of the Fiji software. Cell types were defined based on their relative position and morphology in the confocal/2p image stacks as follows: microglia were characterized as ramified cells located in the parenchyma, perivascular macrophages as elongated cells that follow the outline of a blood vessel, and meningeal macrophages as cells located above the parenchyma and below the dural surface. To define cell migration, cell somata were first outlined and the geometrical center (centroid) was determined using the Fiji software. Cell displacement was then calculated as the vector of the centroid-movement along the x and y axis over 1 h and expressed in μ m h⁻¹. To determine the proportion of moving cells in each population, microglial were considered as stationary cells³¹ and the average + 3 s.d. of their cell displacement (which was most likely a result of minor changes in tissue geometry between imaging

time points) was used as a cut-off for the analysis of mM Φ and pVM. For the cell displacement analysis we compared several groups and used a One-way ANOVA with Bonferroni post hoc testing. For image representation both confocal and 2p images have been gamma-adjusted and processed with a despeckling filter using Photoshop software (Adobe). The z-projection and three-dimensional rendering of the confocal image stack shown in **Figure 5b,c** and **Supplementary Movie 1** were performed using IMARIS software (Bitplane). **Supplementary Movie 2** was assembled using Windows Movie Maker (Microsoft). For the cell displacement analysis we compared several groups and used a one-way ANOVA with Bonferroni *post hoc* testing.

Fluorescence microscopy and cell quantifications. After transcatheter perfusion with PBS, brains were fixed for 24 h in 4% PFA, dehydrated in 30% sucrose and embedded in Tissue-Tek O.C.T. compound (Sakura Finetek Germany GmbH). Cryosections were obtained as described previously^{26,51}. Sections were then blocked with PBS containing 5% bovine serum albumin (wt/vol) and permeabilized with 0.1% Triton-X 100 (vol/vol) in blocking solution. Primary antibodies were added over night at a dilution of 1:500 Iba-1 (019-19741, WAKO), 1:1,000 GFP (600-106-215, Rockland Immunochemicals), 1:100 for MHC class II (ab23990, Abcam), 1:400 CD45 (BD Pharmingen), 1:1000 ER-TR7 (ab51824, Abcam), 1:100 CD31 (552074, BD Pharmingen), 1:500 Laminin (L9393, Sigma-Aldrich) at 4 °C. Secondary antibodies were purchased from Thermo Fisher Scientific added as follows: Alexa Fluor 488 1:500, Alexa Fluor 555 1:500 and Alexa Fluor 568 1:500 for 2h at 20–25 °C. Nuclei were counterstained with 4',6-Diamidin-2-phenylindol (DAPI). Images were taken using a conventional fluorescence microscope (Olympus BX-61 with a color camera (Olympus DP71) or BZ-9000 (Keyence, Osaka, Japan) and the confocal pictures were taken with Fluoview FV 1000 (Olympus) using a 20 \times 0.95 NA (XLUMPlanFL N, Olympus).

In general, numbers of Iba-1⁺ cells were quantified on a wide field microscope with a 200 \times magnification (Olympus BX-61 or BZ-9000). Microglia and cpM Φ were normalized to the area of the region of interest measured by using the cell-P software (Olympus) and expressed as cells mm⁻². pVM Φ cell counts were normalized to the vessel area measured by using the cell-P software (Olympus) and expressed either as cells mm⁻². mM Φ were normalized to the length of the subdural meninges indicated by ER-TR7 immunohistochemistry and measured by cell-P software (Olympus) and finally expressed either as cells/mm. To assess M Φ labeling efficacy over time (for fate-mapping studies), YFP⁺ Iba-1⁺ cells were counted and compared to YFP⁻ Iba-1⁺ cells. At least three sections of a minimum of three mice were used for each analysis.

Three-dimensional reconstruction. Free-floating 40–50- μ m cryo sections from adult brain tissue were stained overnight with anti-laminin, followed by Alexa Fluor 488-conjugated secondary antibody staining, which was added at a dilution of 1:500 for 4 h at 20–25 °C. Imaging was performed on an Olympus Fluoview FV 1000 confocal laser scanning microscope using a 20 \times 0.95 NA objective (XLUMPlanFL N, Olympus). Z stacks were done with 1.1- μ m steps in z direction, with a xy resolution of 1,024 \times 1,024 pixel. Confocal Z-Stacks were analyzed using IMARIS software 7.6 surface plug-in (Bitplane).

Electron microscopy. Animals were killed and transcatheterially perfused with PBS followed by 4% PFA (Serva) and 0.1% glutaraldehyde (vol/vol) (Serva) in PBS, precisely adjusted to pH 7.4. Following removal of the brain, the tissue was kept in the same fixative for 3–6 h followed by thorough rinsing in PBS and preparation of 60- μ m consecutive sections using a vibrating microtome (Leica Microsystems). The sections were blocked with 3% of bovine serum albumin (Sigma-Aldrich) in Tris-buffered saline (TBS-BSA) followed by incubation of the primary antibody (goat anti GFP, 1:200, Acris antibodies) in TBS-BSA over night at 4 °C. After thorough rinsing, sections were incubated with biotinylated secondary antibodies (rabbit anti goat, 1:250, Sigma-Aldrich) in TBS-BSA for 2 h. After further rinsing, the sections were incubated with ExtrAvidin (1:100, Sigma-Aldrich) for 1 h and were finally stained with diaminobenzidine (Sigma-Aldrich) to achieve an electron dense precipitate allowing detection at the level of light as well as electron microscopy. Sections were further stained with 0.5% osmium tetroxide (vol/vol) (EMS) and 1% uranyl acetate (wt/vol) (Serva), dehydrated and embedded between coated microscope slides and cover glasses using Durcupan (Sigma-Aldrich) followed by polymerization at

56 °C for 48 h. After identification of the respective cells by light microscopy the sections were trimmed and transferred on blocks of resin for ultra-thin sectioning using an ultra-microtome (Leica Microsystems). Ultra-thin sections of 55-nm thickness were transferred on formvar-coated copper grids, stained with lead-citrate (Sigma-Aldrich) and analyzed using a Zeiss Sigma electron microscope (Zeiss NTS).

Flow cytometry. After transcardial perfusion with PBS, brains were homogenized with a potter in. Whole-brain homogenate was separated by 70/37/30% layered Percoll gradient centrifugation at 800 g for 30 min at 4 °C (no brake). The CNS macrophages containing interphase was then collected and washed once with PBS before staining. BM monocytes were isolated from tibia and femur before staining. Cells were stained with primary antibodies directed against CD11b (M1/70), CD36 (No.72-1), CD45 (30-F11), CD115 (AFS98), F4/80 (BM8) (eBioscience), CD64 (X54-5/7.1), Ly6C (AL-21) (BD Biosciences) and MHC II (M5/114.15.2) (BioLegend) at 4 °C for 20 min. Cells were washed and analyzed using a FACS Canto II (BD Biosciences) or sorted using a MoFlo Astrios (Beckman Coulter). Viable cells were gated by physical forward and side scatter pattern. Data were acquired with FACSDiva software (Becton Dickinson). Postacquisition analysis was performed using FlowJo software, version 7.6.5 (Tree Star).

Single cell RNA-seq. Microglia and perivascular macrophages were obtained from a thorough preparation of the brain cortex in which meninges and choroid plexus were removed before as described previously¹⁸. In brief, cortex (Bregma, AP: 1.54 to -1.82 mm) was dissociated into a single cell suspension. Mice were deeply anesthetized with a mixture of ketamine/xylazine (80 mg per kg; 10 mg per kg), and the brain was quickly dissected and transferred to ice-cold oxygenated cutting solution (87 mM NaCl, 2.5 mM KCl, 1.25 mM NaH₂PO₄, 26 mM NaHCO₃, 75 mM sucrose, 20 mM glucose, 1 mM CaCl₂, and 2 mM MgSO₄) and kept in the same solution during sectioning on a vibratome (VT1200 S, Leica) in 300- μ m-thick slices. The area was dissected from each slice, and the tissue was dissociated using the papain dissociation system (Worthington) following the manufacturer's instructions. Absence of pia was confirmed by subsequent H&E staining's of tissue specimen. All the solutions were oxygenated for at least 10 min with a mixture of 5% CO₂ in

O₂ (Labline). Oxygenation and a short time of dissection were crucial to keep a high rate of survival in the cell suspension. After this, the cell suspension obtained was filtered with 20- μ m filter (Partec) and kept in cold HBSS solution (SIGMA) with 0.2% BSA and 0.3% glucose. Then the cells were immediately loaded in the C1 chip. Data for pvM Φ and microglia were taken from ref. 18 where they were obtained as part of single-cell analysis of more than 3.000 single cells, of which a small fraction were classified as microglia and pvM Φ . The unbiased *de novo* clustering was described there. Essentially, cells were clustered based on their whole transcriptome profiles, and subsequently clusters were interpreted as cell types by using cluster-specific genes of known function. Cell types were then validated in tissue sections by immunohistochemistry and single-molecule RNA FISH. pvM Φ were validated by Mrc1 and Lyve1 immuno, and microglia were identified by Aif1 (Iba-1) immuno (and being negative for Mrc1 and Lyve1).

Monocytes were isolated from BM by flow cytometry sorting for CD45, CD11b, Ly6C and CD115. Cells were then subjected to single-cell RNA-seq using the C1 AutoPrep instrument (Fluidigm) and STRT/C1 protocol, as previously described¹⁸. Each single cell was imaged and manually curated, and only single healthy-looking cells without debris were used for the analyses. Expression profiles were obtained as absolute cDNA molecule counts, and normalized to transcripts per million to compensate for differences in total transcriptome size between cell types. For t-SNE, we used the first 25 principal components, with perplexity 50 and theta = 0.5. Expressed genes can be found at <http://linnarssonlab.org/cortex/>.

Statistical analysis. Data were tested for normality applying the Kolmogorov-Smirnov test. If normality was given, an unpaired *t* test was applied. If the data did not meet the criteria of normality, the Mann-Whitney *U* test was applied.

49. Misgeld, T., Nikic, I. & Kerschensteiner, M. *In vivo* imaging of single axons in the mouse spinal cord. *Nat. Protoc.* **2**, 263–268 (2007).
50. Romanelli, E. *et al.* Cellular, subcellular and functional *in vivo* labeling of the spinal cord using vital dyes. *Nat. Protoc.* **8**, 481–490 (2013).
51. Goldmann, T. *et al.* USP18 lack in microglia causes destructive interferonopathy of the mouse brain. *EMBO J.* **34**, 1612–1629 (2015).